Proceedings of the 2014 IEEE
International Conference on Robotics and Biomimetics
December 5-10, 2014, Bali, Indonesia

Rapid Prototyping Design and Control of Tensegrity Soft Robot for Locomotion

Kyunam Kim, Adrian K. Agogino, Deaho Moon, Laqshya Taneja,
Aliakbar Toghyan, Borna Dehghani, Vytas SunSpiral, and Alice M. Agogino, *Member, IEEE*

Abstract—Co-robots that can effectively move with and operate alongside humans in a variety of conditions could revolutionize the utility of robots for a wide range of applications. Unfortunately, most current robotic systems have difficulty operating in human environments that people easily traverse, much less interact with people. Wheeled robots have difficulty climbing stairs or going over rough terrain. Heavy and powerful legged robots pose safety risks when interacting with humans. Compliant, lightweight tensegrity robots built from interconnected tensile (cables) and compressive (rods) elements are promising structures for co-robotic applications. This paper describes design and control of a rapidly prototyped tensegrity robot for locomotion. The software and hardware of this robot can be extended to build a wide range of tensegrity robotic configurations and control strategies. This rapid prototyping approach will greatly lower the barrier-of-entry in time and cost for research groups studying tensegrity robots suitable for co-robot applications.

I. INTRODUCTION

Tensegrity structures have a unique design, being constructed by connecting isolated rods with a network of cables (Figure 1a) [1], [2]. When a tensegrity structure is loaded, both types of members bear loads only in axial directions: the bars undergo pure compressive forces and the cables bear pure tensile forces. While none of the rods touch each other, a tensegrity structure is able to maintain an equilibrium geometry, determined by pretensions of the cables.

These naturally compliant tensegrity structures have several unique properties that are advantageous for co-robotic or soft robotic platforms that can safely work beside, or cooperatively with people. Tensegrities are (1) structurally compliant, (2) lightweight, (3) robust, (4) energy efficient and (5) capable of a wide range of motions [3]–[6]. The compliance of tensegrity structures give them two large advantages for co-robotics and soft robotic applications: (1) They can be hit with significant force or fall from significant distance without sustaining serious damage, since the structure tends to deform on impact, therefore absorbing shock; (2) Accidental impact with a human causes minimal harm as the structure absorbs most of the

K. Kim, D. Moon, L. Taneja, A. Toghyan, B. Dehghani, A. M. Agogino are with the Department of Mechanical Engineering, University of California at Berkeley, Berkeley, CA 94720 USA (e-mail: knkim@berkeley.edu; dmoon@berkeley.edu; laqshya_taneja@berkeley.edu; aliakbar_toghyan@berkeley.edu; borna2467@berkeley.edu; agogino@berkeley.edu).

A. K. Agogino is with the University of California at Santa Cruz, Santa Cruz, CA 95064 USA, and also with the NASA Ames Research Center, Moffett Field, CA 94035 USA (e-mail: adrian.k.agogino@nasa.gov).

V. SunSpiral is with Stinger Ghaffarian Technologies, Inc., Greenbelt, MD 20770 USA, and also with the NASA Ames Research Center, Moffett Field, CA 94035 USA (e-mail: vytas.sunspiral@nasa.gov).
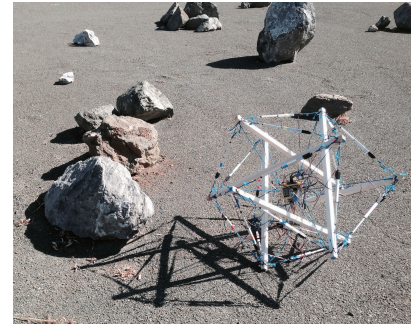
(a)

(b)

Fig. 1. (a) Rapidly prototyped tensegrity robot shown in the NASA Ames RoverScape. (b) Detailed view of rod, cable and actuator connections.

shock. Currently, tensegrity structures are most commonly sold as toys for infants due to these safety properties.

Tensegrity robots have been envisioned for assistive and rehabilitative healthcare by providing hospital service or direct in-home assistance. If these uniquely deformable robots are equipped with locomotion ability, they may be able to move supplies or medicine, concentrated in their central protected payloads, to doctors and patients around the hospital. Tensegrity robots have also been proposed for rough and unstructured terrains such as construction settings and search and rescue. NASA (U.S. National Aeronautics and Space Administration) is exploring tensegrity robots for planetary space exploration as autonomous vehicles or co-robots working with astronauts [7], [8].

Despite the benefits and prominent applications, only a few tensegrity robots have appeared in the prior literature. Possible reasons include the following:

- Tensegrity robots are mechanically complex and challenging to build.
- Their design requirements differ radically from traditional robots, and this design space is not yet well understood.
- Accurate control of tensegrity geometry is difficult due to the interaction of forces and positions between members.
- There are no standardized components for building tensegrity robots, making them expensive to build.

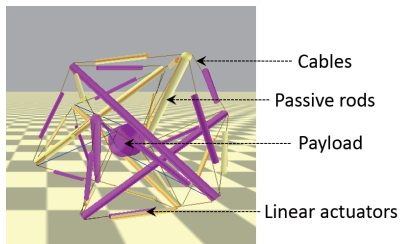The ultimate goal of our research is to overcome the above

Fig. 2. Rapidly prototyped tensegrity robot simulated in the NTRT.

difficulties, and develop a *rapid prototyping kit* from which various tensegrity robotic configurations can easily be built (with differing numbers of rods, cables, actuators and sensors). We anticipate that the kit will not only foster research on tensegrity robots but also will aid young students to get familiarized with tensegrities.

We present our easy-to-build and modularly designed tensegrity robot along with an open-loop control method for locomotion, resulting in the following advantages:

- Rapid to prototype, only two hours to build the robot.
- Mainly built with off-the-shelf components, reducing the overall cost and complexity of the system.
- Lightweight – the total weight of the robot is 2.7 kg.
- Completely untethered and self-sustaining.
- Simple system architecture allows easy diagnostics and quick fix of problems.
- Simple, unified control input generates various motions.
- Easily programmable with icon-based interface.

A. Prior Research

Buckminster Fuller [1] coined the term tensegrity as a portmanteau of "tensional integrity". Much of the prior work on tensegrities has focused on structural issues. Some of this research was additionally motived by tensegrity structures in nature [9]–[11]. The artist Kenneth Snelson was interested in art and nature and created artistic renditions of biomimetic tensegrity structures [12], [13]. Other researchers focused on form-finding techniques [14]–[16] and the design and analysis of static structures [5], [17], [18].

Research on utilizing tensegrity structures for locomotor robots is relatively recent with initial efforts at formalizing the dynamics of tensegrity structures [5], [19]–[22]. Tur and Juan discuss how the complex compliance, multi-path load distribution and non-linear dynamics pose challenges to traditional control approaches [23]. Paul et al. used simplistic actuators for testing a slow-walking robot on flat, unobstructed ground [24]. Böhm et al. presented two locomotion systems based on tensegrity structures with a minimal number of struts [25]. Spine-like tensegrity structures constructed by connecting multiple segments of simpler tensegrity structures together was shown to be capable of locomotion on uneven terrains [11]. Another tensegrity robot with two linked segments was developed for exploring duct systems [26].

The rapid prototyped tensegrity robot described herein is specifically based on a 6-rod tensegrity structure. Shibata and Hirai formerly built this type of robot using shape memory alloy coils as actuators [27]. This robot was improved later to use pneumatic actuators [28], [29], but this required a tethered external power source for the robot's operation. Another robot design involved attachment of three vibration DC motors at the midpoints of three out of six rods [30]. The robot was controlled to move by exciting itself with the motors operating at different frequencies.

Ongoing work at the NASA Ames Research Center has begun developing a more advanced version of a spooled-cable actuation system for autonomous space exploration [26], [31]–[34]. This system is heavier than would be desirable as a co-robot due to the need to carry a heavy payload of scientific instruments, and to survive significant impact shocks of landing and high-speed dynamic locomotion. Moreover, the system entails highly integrated sensors and a distributed control system, making it laborious to construct a prototype. This motivated our development of a rapid prototyping tensegrity robot for constructing and testing tensegrity structures and control strategies for broader co-robotic applications.

B. Our Contribution

In this paper, we introduce our low-cost and rapidly prototyped tensegrity robot, and utilize a greedy search algorithm to find an open-loop control strategy for the robot's gait production. Specifically, the robot is designed and manufactured based on a 6-rod tensegrity structure (Figure 2) which has a geometry similar to an icosahedron. The highly symmetric geometry of the robot greatly simplifies the development of an open-loop control strategy. Our greedy search approach intends to choose an actuation policy that reduces and zeroes the distance between the robot's ground projected center of mass and the supporting polygon edge about which the robot will rotate. The control strategies were developed in simulation and then tested on the rapidly prototyped robot hardware. We also demonstrated in hardware that the tensegrity robot can perform a number of motion maneuvers, such as forward locomotion and turning left and right.

II. ROBOT STRUCTURE

There are a wide range of ways to connect rods and cables to construct a tensegrity structure. Our robot is based on the tensegrity structure which consists of 6 rods and 24 cables (Figure 2). Each rod end is connected to 4 cables to create a structure with 8 equilateral triangles and 12 isosceles triangles formed by the positioning of the rod ends or *nodes*. Since there is not a cable connecting every node (6 are missing – one between each parallel rod end), each of the isosceles triangles also presents itself as an *open triangle* with cables connecting two of its three edges. Meanwhile every equilateral triangle is a *closed triangle* with cables connecting all three of its edges. Throughout this paper, the triangle in contact with the ground is referred to as the *base triangle*.

While a traditional tensegrity structure does not include a *payload*, which is a functional load in the center of the structure, our robot is designed to have a controller unit as

TABLE I
PHYSICAL PARAMETERS OF ROBOT

Total robot mass	2.7 kg
Rod length	0.69 m
Rod mass	94.63 g
Outer cable rest length (looped)	3.8 cm
Inner cable rest length	35 cm
Cable stiffness (looped)	1193 N/m
Payload mass	785 g
Actuator mass	56 g
Actuator stroke length	10 cm
Actuator speed	5 mm/s
Actuator body length (fully retracted, with spring snaps)	20 cm

Fig. 3. 2D conceptual diagram of different stages of a step. (a) At rest. (b) Deformation. (c) Rotation. (d) Strike. (e) Recovery.

a payload. This adds mass to the structure and thus changes the deformation properties of the structure. Whereas the cables connecting nodes in the outer structure are referred to as *outer cables*, the cables keeping the payload inside of the structure are called *inner cables* (See Figure 2).

Structurally deforming a tensegrity structure by changing the length of the outer cables such that the ground projection of the robot's center of mass (*GCoM*) escapes a supporting polygon will result in a rotation or a discrete *step* from one base triangle to another. A detailed discussion of steps is presented in Section IV.

III. HARDWARE DESIGN

In the following, we present the mechanical design of our lightweight rapid prototyping tensegrity robot with untethered, fully actuated (i.e., all of its outer cables are actuated) capabilities.

A. Rod Design

The overall size of the robot is determined by the length of a rod. The length of each rod in our robot is determined by the ratio of the actuator's stroke length to the length of a rod. Simulations predict that 10% actuation range relative to the rod length was sufficient to generate locomotion from a 6-rod tensegrity robot [35]. In our robot, the rod length is 0.69 m, and the ratio of actuation range is 14.5%, as our linear actuators have a stroke length of 10 cm. This results in relatively large structural deformation of the robot, making it possible to take a step with only a few actuators. Moreover, the overall robot size is large enough to provide space for a payload at its center.

Together with actuators and a payload, rods are responsible for a significant portion of the weight of the robot. As an effort to reduce the weight of the robot, lightweight balsa wood is chosen for the rod material. Although other materials such as bamboo and carbon fiber are considered, the advantages of balsa wood include low price, relatively light weight, and easy machinability. The ends of the rods are drilled with holes for cable connection and saturated with epoxy to help tolerate the tension from the connected cables.
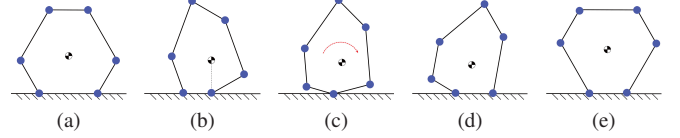
B. Cable Selection and Linear Actuator Attachment

Elastic cords with a thickness of 3.18 mm are used as cables due to their linear elasticity and shock absorption properties. To apply forces to the robot's outer cables, 24 linear actuators (Firgelli L12-R) are placed at the middle of the outer cables (Figure 1b). The linear actuators have a stroke length of 10 cm, and can provide up to 45 N of force, reaching a maximum speed of 5 mm/s. The maximum force provided by the linear actuators is well above the maximum force required to pull the outer cables to their maximum stretched length.

For easy connection of the linear actuators to the outer cables, spring snaps are used between them. The outer cables are looped around the snaps, looped through the cross holes of the rod ends, and then fixed with a hog ring in order to ensure a secure connection and minimize dead length. Reducing dead length allows actuator retraction to focus more towards structure deformation rather than towards cable tensioning. The hog rings also help to connect all the outer cables in even lengths such that their tensions are equally distributed when the robot is not deformed. In the cable operation region, the effective stiffness of the looped cables is experimentally measured to be linear with a spring constant of about 1,193 N/m.

C. Payload Attachment

Our robot carries a controller and other electronic components required to control the actuators as a payload. Specifically, the payload is composed of a controller brick (LEGO Mindstorms EV3), Li-Ion batteries (Tenergy), and servo controllers (Mindsensors) to control the linear actuators. If needed, additional scientific payloads may also be added. The same elastic cords used for outer cables are also used to connect the payload. A total of 12 cables are used for payload connection in a way that one end of each inner cable is connected to one of the nodes, while the other end is connected to the payload by a spring snap. The rest lengths of these inner cables are set to 35 cm such that the payload is located close to the center of the structure and so that the tension is primarily concentrated in the inner cables connected to the nodes of the top-facing triangle above the base triangle. The payload weighs 785 g and accounts for a large portion of the robot's total weight of 2.7 kg. It is critical to control the centered-placement and loading provided by the payload to maintain symmetry and predictability of motion. The physical parameters of the robot are summarized in Table I.

IV. CONTROL STRATEGY

The robot's locomotion can be broken down into a sequence of steps. For our tensegrity robot, a step consists of 5 different stages (Figure 3):

1) *At rest:* The robot is initially undeformed and at rest.
2) *Deformation:* The robot deforms until its GCoM escapes current base triangle.
3) *Rotation:* Rotation about one edge of the base triangle.
4) *Strike:* The robot lands on the next base triangle.
5) *Recovery:* The robot recovers to an undeformed state, preparing for the next step.

Due to the highly symmetric nature of a 6-rod tensegrity structure, motion possibilities can be generalized for the triangle classes described in Section II. Within the structure, each closed triangle is surrounded by three open triangles, while each open triangle is surrounded by two closed triangles and one open triangle. As a result, when starting on a closed base triangle, the robot could only rotate onto one of three surrounding open base triangles with a single step. On the other hand, when starting on an open base triangle, the robot could land on either one of the two neighboring closed base triangles or an open base triangle. In summary, three different types of locomotion steps are considered herein:

- *CO-step* leads the robot from a closed base triangle to an adjacent open base triangle.
- *OC-step* leads the robot from an open base triangle to an adjacent closed base triangle.
- *OO-step* leads the robot from an open base triangle to an adjacent open base triangle.

A similar classification of steps is also presented in [28], [29]. While similar, our robot extends their work by being untethered and carrying a payload, which changes the dynamics of motion. Also, while they experimentally found pairs of actuators that will make a step, we first develop actuation policies in simulation by utilizing a greedy search algorithm, and then implement and verify the controllers on the hardware. By taking this approach, we are able to quickly identify new actuation policies whenever there is a hardware change, successfully meeting the concept of rapid prototyping. Moreover, our actuation policies are not limited to include two actuators. However, because we are using a greedy approach, we only find a single actuation policy per running of the algorithm, while [28], [29] found all possible pairs of actuators resulting in a step.

In the following, we discuss the approach taken to search for actuation policies for CO-, OC- and OO-steps of the robot. In our robot, the outer cables are actuated with the linear actuators to deform the structure in a desired way. All the linear actuators are fully extended initially, and the actuation policies identify subsets of the actuators that will achieve one or more steps if fully retracted in phase. Furthermore, we only consider steps on a flat ground in this work, although the approach presented below can also be applied to other elevation conditions and terrains.
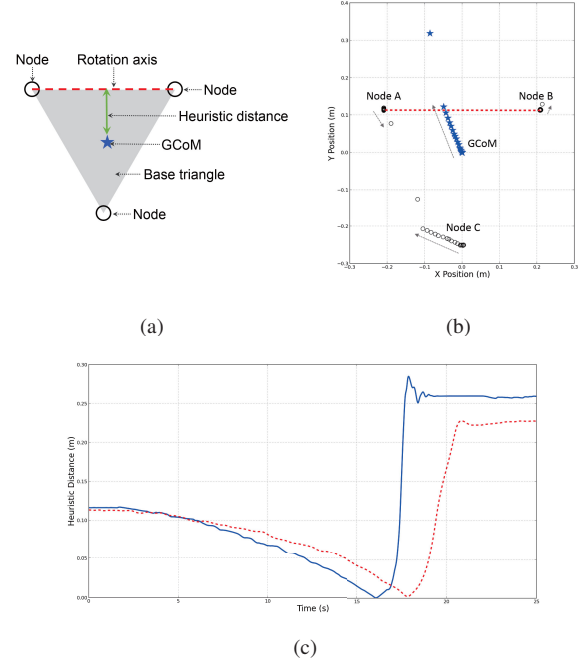

(a)

(b)

(c)

Fig. 4. (a) Definition of the heuristic distance (about one chosen base triangle edge) used for the search algorithm. (b) Trajectories of the GCoM and ground contacting nodes during a CO-step, tracked with Vicon® system. Markers represent the positions of the GCoM and nodes for every 0.1 seconds. Dashed arrows represent the motion directions of the GCoM and nodes. (c) Change of heuristic distances during a COC-step. Solid and dashed lines represent experiment and simulation results, respectively. The robot starts to rotate as soon as the heuristic distance becomes zero.

A. NASA Tensegrity Robotics Toolkit

The NASA Tensegrity Robotics Toolkit (NTRT) [36] is used to simulate our robot's motions in order to find actuation policies. NTRT was developed to aid and facilitate tensegrity robotics research, and has been recently released as open-source software. Building upon the open-source Bullet Physics Engine [37], NTRT is capable of simulating dynamic behavior of various tensegrity robots and enables validation of different controls. The performance of the simulator has been verified, for instance, in [31] where motions of a tensegrity robot simulated with NTRT are validated with the hardware.

Our robot was simulated using the physical parameters given in Table I, as shown in Figure 2. One difference between the simulation and our hardware is the means of providing forces to the outer cables. In our hardware, each cable is provided with a control force by a linear actuator that is placed in the middle of the cable. While added recently, at the time of this work, NTRT did not model linear actuators. Instead, we changed the rest lengths of the outer cables individually to apply forces to them in the simulation. To match the hardware dynamics, we found a mapping such that the simulated cable forces matched the forces applied by the linear actuators in the hardware.

TABLE II
ACTUATION POLICIES FOUND IN SIMULATION
(SEE FIGURES 5 AND 6 FOR NODE NUMBERING.)

Type of step	Starting triangle	Landing triangle	Actuation policy
CO-step	(0,8,9)	(6,9,11)	(0,9), (5,6), (6,11)
CO-step	(0,8,9)	(6,9,11)	(0,9), (5,6), (10,11)
OC-step	(8,9,11)	(0,8,9)	(6,9)
OC-step	(8,9,11)	(0,8,9)	(8,10)
OO-step	(8,9,11)	(8,10,11)	(8,9), (9,11), (7,10), (1,10), (6,11), (0,8), (1,8), (0,3)

3-tuple: triangle formed by nodes

2-tuple: actuated cable between two nodes

B. Actuation Policy Search for CO-steps

Throughout the work, a greedy search algorithm is used in order to find step-wise actuation policies that will result in one or more steps of the robot from its initial position. Our heuristic for the algorithm is the distance between the robot's GCoM and one of the base triangle's edges serving as the rotation axis of that step (Figure 4a). When the robot is standing on one of its closed triangles, it can make a CO-step in three different directions. Each step uses one of the base triangle's edges as a rotation axis. Because of the 3-fold symmetry of a 6-rod tensegrity structure, actuation policies for the three CO-steps are also expected to be symmetric. Therefore, it suffices to search for actuation policies for only one of the three CO-steps. The actuation policies for the other two CO-steps, and all possible CO-steps, can be easily inferred from this result, as discussed in Section V-A.

The algorithm used to search for actuation policies is as follows: Initially, the robot is set to stand on one of its closed triangles in the simulator and one edge of the base triangle is chosen as a rotation axis for a CO-step to be performed. The goal of the algorithm is to find a subset of the linear actuators that will move the robot's GCoM outside of the base triangle if fully retracted in phase, thus resulting in a step. In other words, the algorithm looks for a combination of linear actuators that will result in zero heuristic distance if all of these are fully retracted. To achieve this, the algorithm runs multiple iterations, adding one actuation to the developing policies in each iteration until the goal is met.

Specifically, during the first round search, each actuator is fully retracted one at a time and the heuristic distance between the GCoM and the rotation axis is measured for each case after the robot settles upon deformation. As expected, none of these initial single actuation trials resulted in a successful step. Next, the actuator which minimizes the heuristic distance is identified as the most promising and is added to the current policy under development, which is initially empty. During the next round, two actuators are fully retracted at a time, one being the previously found best actuator and the others being chosen from the rest of the actuators. Again, none of these double actuation trials satisfied the goal in our simulation. As before, the pair of actuators which resulted in the minimum heuristic distance is identified. The procedure is repeated until the policies meeting the goal are found.
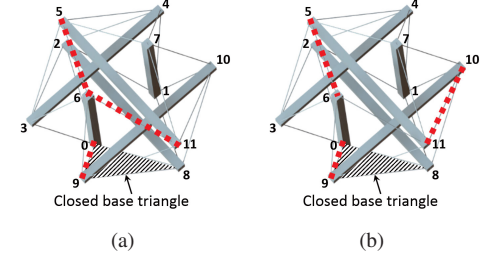

Fig. 5. CO-step policies found in simulation. Hashed triangles and thick dotted lines represent closed base triangles and actuated cables, respectively. Node numbers used in Table II are also shown. (a) CO-Policy 1. (b) CO-Policy 2.
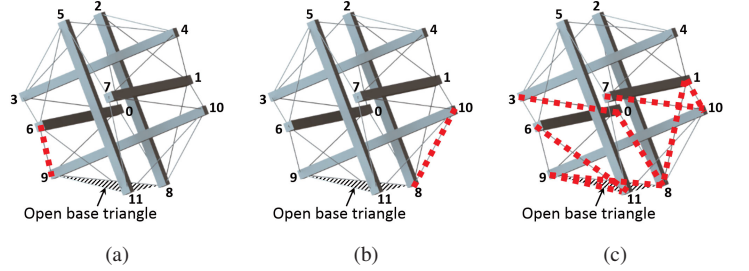

Fig. 6. OC- and OO-step policies found in simulation. Hashed triangles and thick dotted lines represent open base triangles and actuated cables, respectively. Node numbers used in Table II are also shown. (a) OC-Policy 1. (b) OC-Policy 2. (c) OO-Policy.
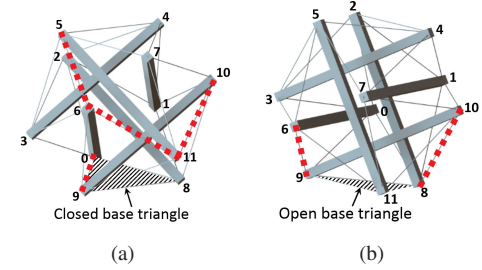

Fig. 7. Updated policies implemented on hardware. Hashed triangles and thick dotted lines represent base triangles and actuated cables, respectively. (a) Updated policy for CO-steps. (b) Updated policy for OC-steps.

After multiple runs of this algorithm, two successful actuation policies were found for a CO-step. Both policies include three different actuators (Table II and Figure 5). When the two actuation policies are applied in the simulation, the robot automatically performs the following OC-step as well, thus arriving at the next closed base triangle. In other words, the goal to achieve a CO-step results in a closed to open to closed base triangle step (COC-step), skipping the recovery stage of the CO-step. This happens because the applied actuation allows the GCoM to additionally cross the narrow width of the open triangle to make the OC-step. The momentum of the robot gained from the CO-step is also providing some assistance.

C. Actuation Policy Search for OC- and OO-steps

Although in most cases the robot motion is designed to land on a closed base triangle during its locomotion, there
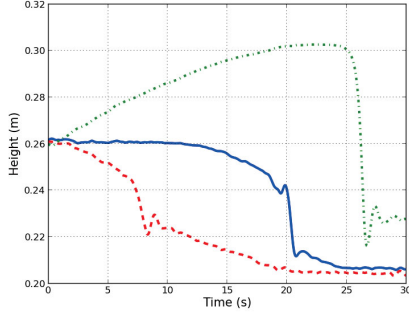
11

Fig. 8. Simulated result of height changes of the robot's center of mass during different types of steps. Solid, dashed, and dotdash lines represent CO-, OC- and OO-steps, respectively. Notice that in order to perform an OO-step, the robot has to overcome a high potential energy barrier. Actuation policies provided in Figures 6c and 7 were used to simulate the steps.

will be situations when the robot will land on an open base triangle due to instabilities or obstacles. Two different types of steps are available from this pose: OC- and OO-steps. We first consider an OC-step. Because the robot possesses bilateral symmetry about its sagittal plane when standing on an open base triangle, it is sufficient to search for actuation policies that would result in an OC-step towards either of the two adjacent closed base triangles.

The same algorithm from Section IV-B is used to find actuation policies to achieve an OC-step. Two successful single-actuator policies are found (Table II and Figure 6), which show that less actuation effort is required to make an OC-step than a CO-step, for which three-actuator policies were found. This is because the closed triangles in the robot structure possess larger areas and thus provide more static balance compared to the open triangles.

For the sake of completeness, an actuation policy for an OO-step was also developed with the same algorithm (Table II and Figure 6c). The actuation policy involves eight actuators and is energy inefficient compared to CO- or OC-steps. For this reason, this policy has not been implemented on our hardware.

D. Energy Efficiency of Steps

In [27], it was shown that the gravitational potential energy change during the three different types of steps was identical, when a non-deforming regular icosahedron tensegrity structure was assumed and rods were only mass components. These assumptions are no longer valid in a realistic robot like we have built, due to the following:

- The robot's geometry is not a regular icosahedron.
- Locomotion is obtained from structural deformation.
- Rods, actuators, and payload account for a large portion of the robot's total weight.

For a more realistic analysis, we have tracked the height change of the robot's center of mass during CO-, OC- and OO-steps in the simulation. The steps are performed using the actuation policies presented in Figures 6c and 7. A detailed discussion of policies in Figure 7 is presented in Section V-A. The result is shown in Figure 8.

Our simulations show that the maximum height difference of the robot's center of mass during an OO-step is larger than with CO- and OC-steps. In other words, the robot has to overcome a higher potential energy barrier when performing an OO-step. In fact, the OO-step policy requires eight actuators, while the CO- and OC-step policies require only three and one actuator(s), respectively. As OO-steps turn out to be energy inefficient, only OC-steps are considered for the hardware movement when starting on an open base triangle. As a result, the robot's most efficient locomotion is a sequence of alternating CO- and OC-steps.

V. EXPERIMENTS

A. Policy Implementation

The actuation policies found with the simulation are implemented and tested on our physical robot. First, the CO-step policies in Table II are extended to cover all possible CO-steps from any closed base triangle. From a set of experiments, however, we observe that while some of these extended policies are successful in making CO-steps, others are marginally unable to rotate the structure – a slight perturbation will initiate the step in some cases. This happens because our algorithm only provides information as to whether a given policy would zero the heuristic distance and allow the robot to make a step. It does not tell us how *reliable* the step will be. Therefore, the algorithm returns the policies that are just enough to cause a step in simulation; such policies might fail in hardware due to the stochastic sensitivity of geometries and environmental conditions. However, when the two CO-step policies found with the simulation (Figure 5) are combined together to create a single policy involving four actuators (two of the actuators are common in both actuation policies, see Figure 7a), the success rate increases.

We then tested this updated CO-step policy on all closed base triangles of the robot. Each possible step (3 from each of the 8 closed triangles) was tested three times to check for consistency. Our experiments show that, as predicted in the simulation, all of the updated CO-step policies are successful in making desired COC-steps (i.e., a CO-step followed by OC-step) for all trials. Snapshots of the robot during a COC-step are presented in Figure 9.

The OC-step policies developed in the simulation (Table II) are also extended to cover all possible OC-steps from any open base triangle and tested with our hardware. As in the previous case, it is observed that some of the extended OC-step policies are successful in making steps, but the rest are marginally unsuccessful in causing rotation. As before, the two OC-step policies found with the simulation (Figure 6) are merged together to create a single policy involving two actuators (Figure 7b), and the modified OC-step policy is extended to cover all other possible OC-steps. Then, all of the updated OC-step policies were implemented on the hardware. Each of the possible OC-steps (2 from each of the 12 open triangles) was tested three times and all trials were successful.

To examine the validity of the applied policies, the motion of the robot during a COC-step was tracked using a
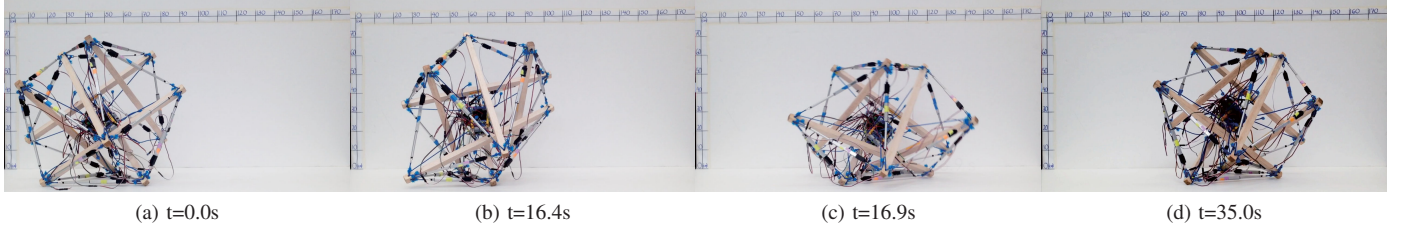
|(a) t=0.0s | (b) t=16.4s | (c) t=16.9s | (d) t=35.0s |

Fig. 9. Different stages of a COC-step of the hardware robot. The robot starts with a CO-step and the following OC-step is automatically performed. (a) Initially at rest. (b) Deformation. (c) Rotation and Strike. (d) Recovery. A full motion video is available at http://best.berkeley.edu/drupal/node/153.
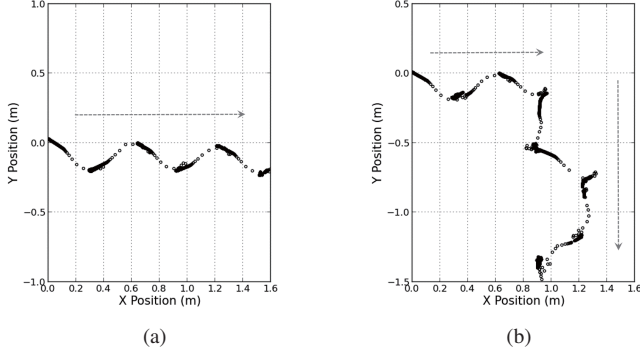

Fig. 10. Trajectories of GCoM tracked with Vicon® system during the robot motions. Markers represent positions of GCoM for every 0.1 seconds. (a) Moving forward. (b) Moving forward and turning right.

Vicon® motion tracking system. The obtained trajectories of the GCoM and base triangle nodes during this step are shown in Figure 4b. The markers in the figure represent the positions of the GCoM and nodes for every 0.1 seconds. Initially, the GCoM is located near the center of the base triangle. During the deformation stage, the GCoM moves towards the rotation axis of the step, reducing the heuristic distance. Node C is also moving towards Node A because the actuator between the two nodes is in action during this step. In fact, among the four actuators included in the modified CO-step policy, simulation results and experiments on the robot identify this actuator as the most critical one for reducing the heuristic distance. The rotation is initiated as soon as the GCoM crosses over the rotation axis. This can be inferred from the large distance between the last two GCoM markers in Figure 4b. The change of the heuristic distance during a COC-step, measured in both simulation and hardware, is shown in Figure 4c.

B. Motion Design

More generalized motions for the robot such as moving forward, turning left, and turning right, have been designed by linking together appropriate COC-steps actuated using our modified CO-step policy. These motions were tracked using a Vicon® motion capture system and the corresponding GCoM trajectories during the motions are shown in Figure 10. In Figure 10a, the robot starts from the origin and performs five COC-steps in a zig-zag fashion about the initialized axis of interest to move forward. For the turning motion in Figure 10b, the robot starts from the origin, first performs three COC-steps to move forward, and makes a turn at its fourth step. The execution of turning motions shows that the robot is steerable, which is desirable when the robot needs to avoid obstacles in co-robotic applications.

VI. Conclusion

In this paper, we present the design of our low-cost, modular, and rapidly prototyped tensegrity robot, based on a 6-rod tensegrity structure. The robot is flexible and lightweight, making it ideal for various co-robotic applications. Unlike conventional tensegrity structures or other tensegrity robots, our untethered robot design also considers a payload installation. By having the payload, the robot is able to perform meaningful tasks such as delivery. We also discuss that the robot's motion can be broken down into three different basic steps. A greedy search algorithm is utilized to determine actuation policies from NTRT simulation for these types of steps. The developed actuation policies demonstrate that more actuation effort is required to perform an OO-step than CO- and OC-steps. For CO- and OC-steps, two policies found with NTRT for each case are combined to generate a more consistently performing policy when tested on the hardware robot. Lastly, we show that different motions (e.g., moving forward and turning) can be developed for different purposes by appropriately connecting discrete steps. The robot's steerability allows it to circumvent obstacles, which is a desirable feature for safe operation in a co-robot environment.

VII. Future Research

At this point, our tensegrity robot is operating on open-loop control for its motion, without any sensor feedback. Future research will test various sensors, such as force sensors at the nodes to measure ground reaction forces, inertial measurement units to measure the pose of the robot, and cameras to detect obstacles. By using the data provided by these sensors, we plan to close the loop in our controller. This will allow the robot to choose and execute step policies on its own, based on its recognized pose and goal. Furthermore, this will allow the robot to autonomously navigate more complex terrain (e.g., move around elevated terrain or climb stairs) and deal with obstacles (e.g., avoid hitting humans). Such functionalities will greatly enhance the robot's performance in co-robotic applications.

The concept of rapid prototyping is expected to play an important role in the future development of the tensegrity robot. Because adding and replacing hardware components of the robot is relatively easy, the time spent in each prototype iteration is minimal. Moreover, the control method we presented in this work can be used to find actuation policies for the updated hardware. In fact, the rapidly prototyped tensegrity robot has already been helpful to NASA in providing a medium for rapidly constructing and modifying configurations and actuation and control strategies for use in their SUPERball robot for planetary landing and exploration [34].

REFERENCES

[1] B. Fuller, "Tensegrity," *Portfolio Artnews Annual*, vol. 4, pp. 112–127, 1961.

[2] A. Pugh, *An introduction to tensegrity*. Univ of California Press, 1976.

[3] R. T. Skelton and C. Sultan, "Controllable tensegrity: A new class of smart structures," in *Smart Structures and Materials' 97*. International Society for Optics and Photonics, 1997, pp. 166–177.

[4] R. E. Skelton, R. Adhikari, J.-P. Pinaud, W. Chan, and J. Helton, "An introduction to the mechanics of tensegrity structures," in *Decision and Control, 2001. Proceedings of the 40th IEEE Conference on*, vol. 5. IEEE, 2001, pp. 4254–4259.

[5] R. Skelton, "Dynamics and control of tensegrity systems," in *IUTAM Symposium on Vibration Control of Nonlinear Mechanisms and Structures*. Springer, 2005, pp. 309–318.

[6] R. E. Skelton and M. C. de Oliveira, *Tensegrity systems*. Springer, 2009.

[7] A. Agogino, V. SunSpiral, and D. Atkinson, "Super Ball Bot – structures for planetary landing and exploration," *NASA Innovative Advanced Concepts (NIAC) Program, Final Report*, Jul. 2013.

[8] V. SunSpiral, G. Gorospe, J. Bruce, A. Iscen, G. Korbel, S. Milam, A. Agogino, and D. Atkinson, "Tensegrity based probes for planetary exploration: Entry, descent and landing (EDL) and surface mobility analysis," *International Journal of Planetary Probes*, 2013.

[9] D. E. Ingber *et al.*, "Cellular tensegrity: defining new rules of biological design that govern the cytoskeleton," *Journal of Cell Science*, vol. 104, pp. 613–613, 1993.

[10] Y. D. Bansod and J. Bursa, "Tensegrity principle based computational model, cytoskeleton," in *Proceedings of The 6th World Conference of the International Association for Structural Control and Monitoring (6WCSCM)*, Barcelona, Spain, Jul. 2014.

[11] B. T. Mirletz, I.-W. Park, T. E. Flemons, A. K. Agogino, R. D. Quinn, and V. SunSpiral, "Design and control of modular spine-like tensegrity structures," in *Proceedings of The 6th World Conference of the International Association for Structural Control and Monitoring (6WCSCM)*, Barcelona, Spain, Jul. 2014.

[12] K. Snelson. [Online]. Available: http://www.kennethsnelson.net/

[13] K. D. Snelson, "Continuous tension, discontinuous compression structures," Feb. 16 1965, US Patent 3,169,611.

[14] M. Masic, R. E. Skelton, and P. E. Gill, "Algebraic tensegrity form-finding," *International Journal of Solids and Structures*, vol. 42, no. 16, pp. 4833–4858, 2005.

[15] C. Paul, H. Lipson, and F. J. V. Cuevas, "Evolutionary form-finding of tensegrity structures," in *Proceedings of the 2005 conference on Genetic and evolutionary computation*. ACM, 2005, pp. 3–10.

[16] A. Tibert and S. Pellegrino, "Review of form-finding methods for tensegrity structures," *International Journal of Space Structures*, vol. 18, no. 4, pp. 209–223, 2003.

[17] N. Bel Hadj Ali, L. Rhode-Barbarigos, A. A. Pascual Albi, and I. F. Smith, "Design optimization and dynamic analysis of a tensegrity-based footbridge," *Engineering Structures*, vol. 32, no. 11, pp. 3650–3659, 2010.

[18] H. Klimke and S. Stephan, "The making of a tensegrity tower," in *IASS 2004 Symposium, International Association for Shell and Spatial Structures*, 2004.

[19] R. Motro, *Tensegrity: structural systems for the future*. Elsevier, 2003.

[20] A. S. Wroldsen, M. C. de Oliveira, and R. E. Skelton, "A discussion on control of tensegrity systems," in *Decision and Control, 2006 45th IEEE Conference on*. IEEE, 2006, pp. 2307–2313.

[21] N. Kanchanasaratool and D. Williamson, "Modelling and control of class nsp tensegrity structures," *International Journal of Control*, vol. 75, no. 2, pp. 123–139, 2002.

[22] H. Murakami, "Static and dynamic analyses of tensegrity structures. part 1. nonlinear equations of motion," *International Journal of Solids and Structures*, vol. 38, no. 20, pp. 3599–3613, 2001.

[23] J. M. Mirats Tur and S. H. Juan, "Tensegrity frameworks: Dynamic analysis review and open problems," *Mechanism and Machine Theory*, vol. 44, no. 1, pp. 1–18, 2009.

[24] C. Paul, F. J. Valero-Cuevas, and H. Lipson, "Design and control of tensegrity robots for locomotion," *Robotics, IEEE Transactions on*, vol. 22, no. 5, pp. 944–957, 2006.

[25] V. Boehm, A. Jentzsch, T. Kaufhold, F. Schneider, F. Becker, and K. Zimmermann, "An approach to locomotion systems based on 3d tensegrity structures with a minimal number of struts," in *Robotics; Proceedings of ROBOTIK 2012; 7th German Conference on*. VDE, 2012, pp. 1–6.

[26] J. M. Friesen, A. Pogue, T. Bewley, M. de Oliveira, R. E. Skelton, and V. SunSpiral, "A compliant tensegrity robot for exploring duct systems," in *Robotics and Automation (ICRA), 2014 IEEE International Conference on*, Hong Kong, Jun. 2014.

[27] M. Shibata and S. Hirai, "Rolling locomotion of deformable tensegrity structure," *Mobile Robotics: Solutions and Challenges (CLAWAR09)*, pp. 479–486, 2009.

[28] Y. Koizumi, M. Shibata, and S. Hirai, "Rolling tensegrity driven by pneumatic soft actuators," in *Robotics and Automation (ICRA), 2012 IEEE International Conference on*. IEEE, 2012, pp. 1988–1993.

[29] S. Hirai, Y. Koizumi, M. Shibata, M. Wang, and L. Bin, "Active shaping of a tensegrity robot via pre-pressure," in *Advanced Intelligent Mechatronics (AIM), 2013 IEEE/ASME International Conference on*. IEEE, 2013, pp. 19–25.

[30] M. Khazanov, B. Humphreys, W. Keat, and J. Rieffel, "Exploiting dynamical complexity in a physical tensegrity robot to achieve locomotion," in *Advances in Artificial Life, ECAL*, vol. 12, 2013, pp. 965–972.

[31] K. Caluwaerts, J. Despraz, A. Işçen, A. P. Sabelhaus, J. Bruce, B. Schrauwen, and V. SunSpiral, "Design and control of compliant tensegrity robots through simulation and hardware validation," *Journal of The Royal Society Interface*, vol. 11, no. 98, 2014. [Online]. Available: http://rsif.royalsocietypublishing.org/content/11/98/20140520.abstract

[32] J. Bruce, K. Caluwaerts, A. Iscen, A. P. Sabelhaus, and V. SunSpiral, "Design and evolution of a modular tensegrity robot platform," in *Robotics and Automation (ICRA), 2014 IEEE International Conference on*, 2014.

[33] A. P. Sabelhaus, J. Bruce, K. Caluwaerts, Y. Chen, D. Lu, Y. Liu, A. K. Agogino, V. SunSpiral, and A. M. Agogino, "Hardware design and testing of SUPERball, a modular tensegrity robot," in *Proceedings of The 6th World Conference of the International Association for Structural Control and Monitoring (6WCSCM)*, Barcelona, Spain, Jul. 2014.

[34] J. Bruce, A. Sabelhaus, Y. Chen, D. Lu, K. Morse, S. Milam, K. Caluwaerts, A. Agogino, and V. SunSpiral, "SUPERball: Exploring tensegrities for planetary probes," in *Proceedings of 12th International Symposium on Artificial Intelligence, Robotics and Automation in Space (i-SAIRAS 2014)*, Montreal, Canada, Jun. 2014.

[35] A. Iscen, A. Agogino, V. SunSpiral, and K. Tumer, "Robust distributed control of rolling tensegrity robot," in *The Autonomous Robots and Multirobot Systems (ARMS) Workshop at AAMAS*, vol. 2013, 2013.

[36] NASA tensegrity robotics toolkit. [Online]. Available: http://irg.arc.nasa.gov/tensegrity/NTRT/

[37] Bullet. Bullet physics simulator. [Online]. Available: http://www.bulletphysics.org/